Tortuosity of Coronary Bifurcation as a Potential Local Risk Factor for Atherosclerosis: CFD Steady State Study Based on *In Vivo* Dynamic CT Measurements

M. Malvè[1,2,3], **A. M. Gharib**[4], **S. K. Yazdani**[5], **G. Finet**[6], **M. A. Martínez**[2,3], **R. Pettigrew**[4], **J. Ohayon**[7,8]

[1]Department of Mechanical Engineering, Energetics and Materials, Public University of Navarra, Campus Arrosadía, 31006 Pamplona, Spain

[2]Aragón Institute of Engineering Research, University of Zaragoza, Zaragoza, Spain

[3]CIBER-BBN, Centro de Investigatión en Red en Bioingeniería, Biomateriales y Nanomedicina, Madrid, Spain

[4]Laboratory of Integrative Cardiovascular Imaging Science, National Institute of Diabetes Digestive and Kidney Diseases, National Institutes of Health, Bethesda, MD, USA

[5]Department of Mechanical Engineering, University of South Alabama, Mobile, AL, USA

[6]Department of Hemodynamics and Interventional Cardiology, Hospices Civils de Lyon and Claude Bernard University Lyon 1, INSERM Unit 886, Lyon, France

[7]Laboratory TIMC-DyCTiM, UJF, CNRS UMR 5525, In3S, Grenoble, France

[8]Engineering School Polytech Annecy-Chambéry, University of Savoie, Chambéry, France

Abstract

The purpose of the present study was to determine whether *in vivo* bifurcation geometric factors would permit prediction of the risk of atherosclerosis. It is worldwide accepted that low or oscillatory wall shear stress (WSS) is a robust hemodynamic factor in the development of atherosclerotic plaque and has a strong correlation with the local site of plaque deposition. However, it still remains unclear how coronary bifurcation geometries are correlated with such hemodynamic forces. Computational fluid dynamics simulations were performed on left main (LM) coronary bifurcation geometries derived from CT of eight patients without significant atherosclerosis. WSS amplitudes were accurately quantified at two high risk zones of atherosclerosis, namely at proximal left anterior descending artery (LAD) and at proximal left circumflex artery (LCx), and also at three high WSS concentration sites near the bifurcation. Statistical analysis was used to highlight relationships between WSS amplitudes calculated at these five zones of interest and various geometric factors. The tortuosity index of the LM-LAD segment appears to be an emergent geometric factor in determining the low WSS amplitude at proximal LAD. Strong correlations were found between the high WSS amplitudes calculated at the endothelial regions close to the flow divider. This study not only demonstrated that CT

Address correspondence to M. Malvè, Department of Mechanical Engineering, Energetics and Materials, Public University of Navarra, Campus Arrosadía, 31006 Pamplona, Spain. mauro.malve@unavarra.es and jacques.ohayon@imag.fr.

imaging studies of local risk factor for atherosclerosis could be clinically performed, but also showed that tortuosity of LM-LAD coronary branch could be used as a surrogate marker for the onset of atherosclerosis.

Keywords

CFD; Wall shear stress; Hemodynamics; Tortuosity; Coronary bifurcation; Atherosclerosis

INTRODUCTION

Wall shear stress (WSS) is a potent hemodynamic factor in the development of atherosclerotic plaque. Several existing techniques—including intravascular ultrasound (IVUS),[23,35] optical coherence tomography (OCT),[25,40] magnetic resonance imaging (MRI), [24,37] and computer tomography (CT)[9] are routinely used to image coronary plaques. New emerging techniques are now capable of measuring coronary artery blood flow *in vivo*. This was successfully demonstrated by Oshinski's group,[19] as they were able to measure velocity profiles of blood flow in the right, left anterior descending, and left circumflex coronary arteries using phase contrast magnetic resonance imaging (PC-MRI). Such non-invasive measurements provide a powerful tool to initiate computational fluid dynamics (CFD) simulations and permit the quantification of wall shear stress (WSS) amplitude, which has been shown to correlate with the local site of plaque deposition.[39] The development of atherosclerotic plaques near coronary artery bifurcations and more specifically, at sites of low wall shear stress (low-WSS) (i.e., zones where WSS is smaller than approximately 1 Pa), has been well established in literature.[1,4,6,11,17,29] Endothelial shear stress plays an important role in the initiation, growth, and progression of the atheroma lesion.[5,27] Moreover, WSS spatial distribution has been proposed in clinics as robust surrogate marker of arterial regions vulnerable for atherosclerosis.[11] The coronary artery geometry (vessel tortuosity, curvature, lumen area, radius, *etc.*) also plays a direct role in WSS spatial distribution, which can alter the occurrence of plaque formation.[50] Several CFD studies have explored the effects of arterial geometry on shear stress measurements by generating either idealized models[3,38,43,44,48] or imaged-based coronary geometries reconstructed from various imaging modalities including CT,[22] MRI,[14] and IVUS coupled to biplane coronary angiography.[11,39,47] However, these are normally focused only on hemodynamic aspects, evaluating the WSS and trying to correlate it with atheromatous pathologies.[11,21,38] Although idealized geometry studies of arterial bifurcation models were used initially to provide valuable insight to the distribution of shear stress, the need for realistic arterial geometry in predicting sites of atherosclerosis (in a clinical setting) remains necessary.[39,46] Stone *et al.* demonstrated the potential benefit of 3D reconstruction of patient arterial geometry, as they were able to correlate regions of low WSS to the progression of atherosclerosis and outward remodeling.[39] Vessel tortuosity has been associated to abnormal development or vascular disease.[15] With the advance of imaging technology, tortuous vessels can be easily detected and various forms have been reported in clinical researches, most commonly curving/curling, angulation, twisting, looping and kinking vessels.[34,45] While mild tortuosity is a common anomaly without clinical symptoms,[15] severe tortuosity can lead to various serious symptoms. Clinical observations have linked tortuous arteries and

veins to aging, atherosclerosis and hypertension among other diseases.[7,16] However, the mechanisms of tortuous vessel formation and development are still poorly understood.[15] In addition, no studies have been conducted regarding the relationship between physiological tortuosity and atherosclerosis exposure. Only few studies have successfully correlated geometrical factors to hemodynamic quantities. In particular the group of Steinman and coworkers has realized an extensive work in this sense for carotid artery.[8,26,41,42] Therefore, the mechanisms of vessel tortuosity and its relationship with cardiovascular diseae need careful investigation. While many biological, animal and clinical studies have explored the relationship between low-WSS, plaque initiation and lesion location.[5,27,39] to our knowledge no clinical or numerical study has investigated the relationship between WSS amplitude and coronary bifurcation geometric factors—specifically, the relationship of patient-specific left main (LM) coronary bifurcation geometry and hemodynamic forces. Therefore, the goal of the present study is to determine whether *in vivo* arterial geometric factors could be used in clinics to predict the risk of atherosclerosis in distinct sites of coronary bifurcations.

MATERIALS AND METHODS

Study Population, 3D Reconstructions and Geometric Indexes

From a population of coronary disease patients examined by CT (Philips CT 16-channel scanner), subjects with minimal luminal coronary stenosis were identified and were subsequently enrolled for this study. In particular, coronary bifurcation of eight subjects ($n = 8$) were identified. These subjects (6 males and 2 females, mean age 48.8 ± 9 years, range 40–67 years) were patients with percentage of vessel remodeling lower than 40%. Table 1 mentions the presence of plaques at the LM, LAD and LCx branches. Figure 1 presents the 3D reconstructions of the eight coronary bifurcations analyzed in this study. Their geometric features were summarized on Table 1. Our measurements shown that for each patient the sum of the three bifurcation angles remains almost constant and close to 360° (mean $\pm$ SD equal to $357.4 \pm 3.24°$) indicating that at the level of the bifurcation site the three coronary branches LM, LAD and LCx were quasi-coplanar. Therefore, statistical regression analyses were conducted with two angles only, namely α_{bif} and $\alpha_{LM–LCx}$. Based on the findings of Glagov *et al.*,[13] coronaries enlarge in response to lesion growth while atherosclerotic lesion lumen area, on the other hand, remains almost constant until the percentage of vessel remodeling exceeds approximately 40%. Patients with higher vessel remodeling were discarded. Thus, using this set of bifurcations we reconstructed the associated idealized healthy luminal coronary bifurcation geometry for each patient. CFD simulations were then performed on these hemodynamically idealized nonpathological bifurcations (i.e., with normal luminal geometries). This research protocol was approved by the Internal Review Board of NIH Clinical Center and patient consent.

CT Image Analysis: 3D Coronary Bifurcation Reconstruction and Plaque Detection

From each patient's CT images, presence of atheromatous plaque in the LM, LAD and LCx branches was analyzed using imaging Aze software (Aze, Ltd, Tokyo, Japan). From the CT sequence of each patient, the centerlines of the left main (LM), left anterior descending (LAD), and the left circumflex (LCx) arteries, as well as the spatial distribution of the luminal radius, were automatically digitized using Aze software. The centerline of a vessel

was defined as the line which connects the luminal centroids of each 2D vascular cross-section (Fig. 2a). Polynomial interpolations were made on each centerlines to extract the bifurcation point (i.e the intersection point of these three centerlines) needed for the 3D reconstruction process (Fig. 2b). Based on both, diastolic CT images and the results presented by Nissen *et al.*[32] showing that at coronary sites of normal subjects the lumen was nearly circular, 3D reconstructions of the coronary bifurcations were numerically modeled by assuming circular cross-sectional lumen area (Fig. 2b). To avoid all potential computational singularities for our CFD calculations which could be induced by a non uniform surface reconstruction, a *b-spline* surface was created using the 3D CAD software SolidWorks (Dassault Systemes SolidWorks Corp., Waltham, MA, USA) (Fig. 2c). Such reconstructed surfaces exhibit better continuity between adjacent cross-sections.

Quantification of Geometric Indexes

Each 3D coronary bifurcation was subjected to a geometric identification by using similar definitions and approach as described by Lee *et al.*[26] and Thomas *et al.*[41] As illustrated in Fig. 3b, starting from the bifurcation point (P_{bif}) and following the luminal centerlines, the three first circular cross-sections LM0, LAD0 and LCx0 inscribed in each branch LM, LAD and LCx, respectively were drawn. While the geometric indexes were defined on the restricted bifurcation geometry (limited by the cross-sections LM2, LAD2 and LCx2, Fig. 3b), the CFD analysis was performed on the entire coronary bifurcation (Fig. 3a). The length of each arterial branch of the restricted geometry was assigned to be twice the diameter of their first inscribed cross-sections LM0, LAD0 and LCx0 of center CLM0, CLAD0 and CLCx0, respectively. Two angles, the bifurcation angle α_{bif} (i.e., angle between the segments $P_{bif}-C_{LCx0}$ and $P_{bif}-C_{LAD0}$) and the angle between the segments $P_{bif}-C_{LM0}$ and $P_{bif}-C_{Lcx0}$ (α_{LM-LCx}) were then measured (Fig. 3b). Tortuosity was computed for each branch separately and for couples of arterial segments as computed for idealized cerebral arteries by Zakaria *et al.*[48] In particular, two tortuosities namely Tortuosity$_{LM-LAD}$ and Tortuosity$_{LM-LCx}$ were also measured for the arterial segments LM2 + LAD2 and LM2 + LCx2, respectively. Tortuosity index (in %) was defined as the percent ratio $100 \cdot (d/L - 1)$, where *d* is the total length of the coronary artery segment and *L* is the shortest distance (Fig. 3c). Two proximal area ratio indexes AR$_{LAD/LM}$ and AR$_{LCx/LM}$ (in %) were also calculated which corresponded to the ratios ($100 \cdot$ LCx2 section area/LM2 section area) and ($100 \cdot$ LCx2 section area/LM2 section area), respectively. Finally, luminal centerlines were used to calculate the radius of curvature of each branch of the coronary bifurcation. This computation was performed using the aforementioned CAD software SolidWorks selecting in the software tool three consecutive centerline points and selecting the middle one as center of the arch.

Computational Fluid Dynamics

Steady state blood flow was simulated for each coronary bifurcation geometries. The mesh generation was performed using the commercial software Ansys Icem CFD v.14.0 (ANSYS Inc., Canonsburg, PA, USA). All coronary bifurcation geometries were meshed with quadratic tetrahedral finite elements (FE). For each case, approximately 400,000 tetrahedral FE were considered with special refinement near the sites of interests, i.e., around the bifurcation point (Fig. 2d). To find the optimal tetrahedral FE sizes, a sensitivity analysis

was initially performed to evaluate different grid refinements. Velocity profiles at the three coronary branches were computed for different grids and for the geometry of patient #1 in order to get a relation between discretization error and element size, and hence, an estimation of the required element size. Velocity profiles showed to differ less than 3% when computed by means of grids bigger than 400,000 elements so that, for reason of computational time the aforementioned grid was selected for the rest of geometries. The optimal FE sizes obtained were approximately 0.6 and 0.12 mm for the internal volume and sub-endothelial layer, respectively. For the sub-endothelial layer next to the bifurcation zones the FE size was close to 0.2 mm (Fig. 2d). The CFD simulation was performed using a commercially available finite element analysis software ADINA (ADINA *R&D* Inc., Watertown, MA, USA). The blood rheology was assumed Newtonian for this study.[20,21] Johnston *et al.*[20] demonstrated in fact that the effect of non-Newtonian rheology is important only at small velocities. From literature, a blood density of 1008 kg/m^3[33] and blood viscosity of 3.5×10^{-2} Pa s was implemented in the model.[22] As no patient specific coronary flow rate measurements were available, the inlet velocity of the LM branch was computed starting from the coronary flow measured by Sankaranarayanan *et al.*[36] The blood flow velocity was obtained at each branch for each bifurcation using the inlet diameter obtained from of the eight patients and the average measured flow. To estimate the flow-rate in each outlet (LAD and LCx) branch, Murray's law was utilized.[31] The velocity at each outlet was computed using the outlets diameters for each bifurcation. Finally, in order to provide fully developed flow inside each coronary model, a 5-inlet and 15-outlet extensions were added to the three model extremities.[22] Although straight, the extensions facilitate the flow dynamic solution and their influence on the flow and on the WSS would be appreciable only in the regions near the reconstructed model inlet and outlets. In the region of interest, i.e., at the restricted bifurcations, less influence is expected on the hemodynamics variables due to the several diameters which separate the location where the boundary condition are imposed from the location of the bifurcation. Five zones of interest were explored specifically, as they represent areas of low and high shear stress values. From each site of interest five WSS amplitudes were collected: two minima at proximal LAD (region #5, Fig. 3c) and proximal LCx (region #2, Fig. 3c) corresponding to low WSS amplitudes (labeled low-WSS$_{LAD}$ and low-WSS$_{LCx}$, respectively) and three maxima at proximal LAD (region #4, Fig. 3c), proximal LCx (region #3, Fig. 3c) and LM branch (region #1, Fig. 3c) corresponding to high WSS amplitudes (labeled high-WSS$_{LM}$, high-WSS$_{LAD}$ and high-WSS$_{LCx}$, respectively).

Statistical Analysis

To test predictability of WSS amplitude, a linear regression analysis was conducted between sites of interest. Similar regression analysis was then performed for prediction of WSS amplitude based on geometrical indexes. Finally, multiple regression analysis was conducted to estimate the simultaneous effects of all geometrical indexes on WSS amplitude obtained at each site of interest. Only results highlighting relevant predictor variables were presented for the multiple regression study. A commercially available software package (SigmaStat 3.5, Systat Software, Inc., Point Richmond, CA, USA) was used to perform the statistical analysis. Regressions with probability values $p < 0.05$ and correlation coefficient R^2 0.70 were considered statistically significant.

RESULTS

Wall Shear Stress Distribution

Figure 4 illustrates the WSS spatial distributions found near the bifurcation for the eight coronary geometries. Since the CFD results near the bifurcations were similar for all patients, we illustrated in detail the results obtained for Patient #1 (Fig. 5). Figure 5 shows clearly the five distinct regions of low and high WSS concentrations mentioned previously as illustrated on Fig. 3c. These regions are produced by changes in velocity field (compare Figs. 5b and 5c). From each of these five sites, the lowest (in regions #2 and 5, see Figs. 3c and 5c) and the highest (in regions #1,3 and 4, see Figs. 3c and 5c) values of WSS were extracted. As expected, the anatomical sites predisposed for atherosclerotic development— i.e., at the level of the bifurcation in the LM region #2 and LCx region #5 (Fig. 5) displayed low values of WSS (i.e., WSS values in the range 0–0.6 Pa). Moreover, three high WSS regions (i.e., WSS values in the range 1.5 to 2.5~Pa) were observed at the level of the bifurcation: in the LM, proximal LCx and proximal LAD segments (i.e., regions #1, 3 and 4 on Fig. 3c).

Correlation Between WSS and Anatomical Coronary Bifurcation Features

The performed statistical analysis revealed a significant correlation ($R^2 = 0.719$ and $p = 0.008$) between the amplitude of the low WSS at the proximal LAD region (low-WSS_{LAD}) and the tortuosity of the LM-LAD segment (Tortuosity LM-LAD) (Fig. 6), but not with branch angles, cross-sectional area ratios, vessel radius and radius curvature. A weak correlation ($R^2 = 0.421$ and $p = 0.082$) was found between the low WSS amplitude computed at the proximal LCx (low-WSS_{LCx}) and the tortuosity of the LM-LCx segment (Tortuosity$_{LM-LCx}$). No correlation was highlighted between the low-WSS_{LCx} and the other geometric bifurcation indexes defined in this study. Strong correlations ($R^2 > 0.9$ and $p < 0.0002$) were found between the amplitudes of the WSS computed at high WSS regions (i.e., between high-WSS_{LM}, high-WSS_{LAD} and high-WSS_{LCx}) (Table 2). Moreover, the performed multiple regressions indicated significant correlations ($R^2 > 0.7$ and $p < 0.01$) between these three high WSS amplitudes and the two angles of the bifurcation, namely: the bifurcation angle α_{bif} and the LM-LCx segment angle α_{LM-LCx} (Table 3).

DISCUSSION

Studies performed by Fry,[10] Caro *et al.*,[2] and more recently Malek *et al.*[29] highlighting the role of WSS, a decisive hemodynamic factor in the development of atherosclerotic plaque, has prompted several CFD simulations, animal experiments, clinical investigations, and biomechanical studies to investigate the role of WSS distributions in coronary branch disease.[5,11,17,38,39] CFD is by now a recognized tool for improving our understanding of vascular flow. Quantifying WSS in normal and pathological disease arteries is a crucial step in predicting the risk of atherosclerosis and plaque progression.[4] Although low WSS has historically been viewed as among the factors that are determinants of atherosclerosis, [2,4,10,27,29] no study hitherto has determined the role of coronary geometric factors—at the level of the main left coronary bifurcation—in the risk of atherosclerosis. The present study, based on a combined clinical and computational approach, investigated the biomechanical

interaction between several geometric bifurcation indexes and WSS amplitudes in five specific endothelial regions close to the flow divider. One important question was addressed by this investigation: What are the key geometric determinants of local risk factor for atherosclerosis in left main coronary bifurcations that might be measured by clinicians?

Tortuosity of the LM-LAD Segment an Emergent Geometric Factor

The minima of the WSS amplitudes computed in the low WSS concentration site of the proximal LAD of all patients (region #5, Fig. 5) were found in the range 0.001 Pa < low-WSS_{LAD} < 0.6 Pa. The tortuosity index of the LM + LAD arterial segment, rather than area ratio or bifurcation angles, has emerged from the statistical study as the main parameter affecting the WSS amplitude at the proximal LAD region opposite to the flow divider (low-WSS_{LAD}). More importantly, the statistical analysis performed suggested that low-WSS LAD amplitude (unit: Pa) seemed to be predictable by the following simple relationship (R^2 = 0.719, p = 0.008, Fig. 6a):

$$\text{low-WSS}_{LAD} = A \cdot \text{Tortuosity}_{LM-LAD} + B \tag{1}$$

where A and B are two constants equal to −0.064 and 0.404 Pa, respectively. In other words, this result indicates that larger vessel tortuosity, result in smaller amplitude of the low-WSS_{LAD} (Fig. 6a). Interestingly, vessel tortuosity was also found by Steinman's group[26] as an emergent geometric index that can be used to predict disturbed flow in human carotid bifurcations. Previous works had also suggested an important role for area ratios,[26,28] which is contrary to our finding here. Indeed, we did not find any correlation between low-WSS_{LAD} and the measured area ratio indexes $AR_{LAD/LM}$ and $AR_{LCx/LM}$. This may be due to the fact that all our patients had similar area ratio amplitudes (means ± SD equal to 93.77 ± 14.49% for area ratio $AR_{LAD/LM}$ and 69.96 ± 11.26% for area ratio $AR_{LCx/LM}$, Table 1).

WSS Amplitude in the Proximal LCx

Although the statistical analysis revealed no correlation between low-WSS_{LCx} amplitude and the measured bifurcation branch angles (Table 3), we found that, for all the patients, the low WSS amplitudes computed in the high risk site for atherosclerosis of the proximal LCx (region #2, Fig. 3c) ranged from 0.001 to 0.04 Pa. These WSS amplitudes were found always smaller than those computed in the proximal LAD (region #5, Fig. 3c). These results agree with the observation and measurements of Cheruvu et al.[6] indicating clearly that the proximal LCx along with the proximal LAD were the two main zones for atherosclerosis.

Importance of Coronary Branch Angles in Predicting WSS Amplitude

Our data demonstrated that the two bifurcation branch angles α_{bif} and α_{LM-LCx} were not particularly strong predictors of low WSS amplitudes located at sensitive regions #2 and 5, which was consistent with the geometric risk study of Lee et al.[26] While the vessel tortuosity appears to be a determinant geometric index for predicting low WSS at proximal LAD region, the bifurcation branch angles emerged as the main factors affecting the high WSS amplitudes high-WSS_{LM}, high-WSS_{LCx} and high-WSS_{LAD}. All correlation coefficients were found to be positive, indicating that the larger α_{bif} and α_{LM-LCx} angles (or smaller angle between the LM and LAD branches), result in higher values of WSS at concentration

sites #1,3 and 4 (Table 3). Such finding agrees with previous computational models suggesting the important role for LM-LAD branch angle in WSS distribution.[21] Plaque occurs also at LM sites where WSS amplitude was found significant [CT images revealed the presence of small plaques in the LM branch on almost all analyzed subjects (Table 1)]. Since the amplitude of the WSS are high (>1.5 Pa) at such locations (Figs. 4 and 5), it is legitimate to think that other factors could be involved in the atherosclerosic process. In other words, low WSS may not be the only unique factor responsible for atherosclerosis. A recent *in vivo* study has demonstrated the possible role of strain distribution, as they were able to show that low intimal strain distribution colocalize with regions of low WSS.[12] Such a study highlights the importance of simultaneous modeling of strain and shear stress in studying arterial disease, and predicting sites of the complex biological process of atherosclerosis.[27]

Study Limitations

Although this study presents original and potentially promising concepts for identification of atherosclerosis sites, several limitations exists. First, all CFD simulations were performed under steady and not pulsatile flow conditions. Although the physics of pulsatile flow differs from steady flow, the study by Soulis *et al.*[38] demonstrated that steady flow assumption did not significantly alter the general flow pattern of their CFD results, and thus will not affect the sensitivity of identified emergent geometric factors to WSS amplitude highlighted in this study. While the spatial distribution of the WSS is essentially not affected by the consideration of steady state simulations, it has to be noted that the computed values may differ from those computed through an unsteady state analysis. These differences are especially important for the maximal WSS which strongly depends on the coronary peak flow of the cardiac cycle. Finally, steady state simulations do not allow the evaluation of indexes such as time average wall shear stress (TAWSS) or oscillatory shear index (OSI) which nowadays are progressively taken importance for coronary hemodynamics. Correlation between these indexes and atherosclerotic plaque locations are out of the aim of this work and are left for further investigations. Second, although our simulations were based on real coronary bifurcations derived *in vivo* from CT scans, the arterial wall was simplified to be rigid and the effects of cardiac motion on the coronary artery hemodynamics was neglected.[49] Finally, a small number of patients were considered in this work. Further studies are needed to extend and strengthen the current finding. Especially the mathematical relation between the low WSS and the tortuosity of the segment WSS_{LAD} we found has to be carefully considered due to the aforementioned aspects.

Relevance for other Clinical Applications

Identification of high risk zones for atherosclerosis will lead to future advances in vulnerable plaque detection technology and potentially to locally oriented preventive strategies. Although, further studies are needed to extend the current work, our results could explain why subjects with more pronounced coronary tortuosity, which is the case for pathophysiology of chronic pressure and volume overload, are more sensitive to atherosclerosis diseases.[18]

CONCLUSIONS

CFD simulation coupled with computer tomography were used to investigate the influence of some geometrical factors of the coronary hemodynamics. The influence of the curvature ratio, area ratio, tortuosity of separated and coupled coronary branches and bifurcation angles on the WSS amplitude was analyzed. Statistical analysis for the eight bifurcations was carried out in order to determine whether these bifurcation geometric factors would allow the prediction of atherosclerosis risk. Tha main finding is that the tortuosity index of the LM-LAD segment appears to be an emergent geometric factor in determining the low WSS amplitude at proximal LAD. In fact, we found strong correlation between the high WSS amplitudes calculated at the endothelial regions close to the flow divider. On the contrary, other factors which have been considered relevant in other studies could not be related with prediction of atherosclerosis risk. This work showed that the tortuosity of the LM-LAD coronary branch could be used as a surrogate marker for the onset of atherosclerosis.

ACKNOWLEDGMENTS

ABBREVIATIONS

$AR_{LAD/LM}$	Area ratio = LAD2 section area divided by LM2 section area
$AR_{LCx/LM}$	Area ratio = LCx2 section area divided by LM2 section area
CFD	Computational fluid dynamics
WSS	Wall shear stress
High-WSS$_{LAD}$	Highest WSS amplitude at proximal LAD (region #4, Fig. 5)
High-WSS$_{LCx}$	Highest WSS amplitude at proximal LCx (region #3, Fig. 5)
High-WSS$_{LM}$	Highest WSS amplitude at the LM site of interest (region #1, Fig. 5)
LAD	Left anterior descending artery
LCx	Left circumflex artery
LM	Left main artery

Low-WSS$_{LAD}$	Lowest WSS amplitude at proximal LAD (region #5, Fig. 5)
Low-WSS$_{LCx}$	Lowest WSS amplitude at proximal LCx (region #2, Fig. 5)
P_{bif}	Coronary bifurcation point
PLS	Percentage luminal stenosis
Tortuosity$_{LAD-LCx}$	Tortuosity of the LAD + LCx arterial segment near the bifurcation
Tortuosity$_{LM-LAD}$	Tortuosity of the LM + LAD arterial segment near the bifurcation
Tortuosity$_{LM-LCx}$	Tortuosity of the LM + LCx arterial segment near the bifurcation
$\alpha_{LM–LCx}$	Angle between LM and LCx branches (unit: °)
$\alpha_{LM–LAD}$	Angle between LM and LAD branches (unit: °)
α_{bif}	Bifurcation angle defined as the angle between LAD and LCx branches (unit: °)

REFERENCES

1. Caro CG, Fitz-Gerald JM, and Schroter RC. Arterial wall shear and distribution of early atheroma in man. Nature 223:1159–1160, 1969. [PubMed: 5810692]

2. Caro CG, Fitz-Gerald JM, and Schroter RC. Atheroma and arterial wall shear. Observation, correlation and proposal of a shear dependent mass transfer mechanism for atherogenesis. Proc. R. Soc. Lond. B Biol. Sci 177:109–159, 1971. [PubMed: 4396262]

3. Chaichana T, Sun Z, and Jewkes J. Computation of hemodynamics in the left coronary artery with variable angulations. J. Biomech 44:1869–1878, 2011. [PubMed: 21550611]

4. Chatzizisis YS, Coskun AU, Jonas M, Edelman ER, Feldman CL, and Stone PH. Role of endothelial shear stress in the natural history of coronary atherosclerosis and vascular remodeling: molecular, cellular, and vascular behavior. J. Am. Coll. Cardiol 49:2379–2393, 2007. [PubMed: 17599600]

5. Cheng C, Tempel D, van Haperen R, et al. Atherosclerotic lesion size and vulnerability are determined by patterns of fluid shear stress. Circulation 113:2744–2753, 2006. [PubMed: 16754802]

6. Cheruvu PK, Finn AV, Gardner C, et al. Frequency and distribution of thin-cap fibroatheroma and ruptured plaques in human coronary arteries: a pathologic study. J. Am. Coll. Cardiol 50:940–949, 2007. [PubMed: 17765120]

7. Del Corso L, Moruzzo D, Conte B, Agelli M, Romanelli AM, Pastine F, Protti M, Pentimone F, and Baggiani G. Tortuosity, kinking, and coiling of the carotid artery: expression of atherosclerosis or aging? Angiology 49:361–371, 1998. [PubMed: 9591528]

8. Ethier CR, Prakash S, Steinman DA, Leask RL, Couch GG, and Ojha M. Steady flow separation patterns in a 45 degree junction. J. Fluid Mech 411:1–38, 2000.

9. Fayad ZA, Fuster V, Nikolaou K, and Becker C. Computed tomography and magnetic resonance imaging for noninvasive coronary angiography and plaque imaging: current and potential future concepts. Circulation 106:2026–2034, 2002. [PubMed: 12370230]

10. Fry DL Acute vascular endothelial changes associated with increased blood velocity gradients. Circ. Res 22:165–197, 1968. [PubMed: 5639037]

11. Gijsen FJ, Wentzel JJ, Thury A, et al. A new imaging technique to study 3-D plaque and shear stress distribution in human coronary artery bifurcations in vivo. J. Biomech 40:2349–2357, 2007. [PubMed: 17335832]

12. Gijsen FJ, Wentzel JJ, Thury A, et al. Strain distribution over plaques in human coronary arteries relates to shear stress. Am. J. Physiol. Heart Circ. Physiol 295: H1608–H1614, 2008. [PubMed: 18621851]

13. Glagov S, Weisenberg E, Zarins CK, Stankunavicius R, and Kolettis GJ. Compensatory enlargement of human atherosclerotic coronary arteries. N. Engl. J. Med 316:1371–1375, 1987. [PubMed: 3574413]

14. Goubergrits L, Kertzscher U, Schoneberg B, Wellnhofer E, Petz C, and Hege HC. CFD analysis in an anatomically realistic coronary artery model based on non-invasive 3D imaging: comparison of magnetic resonance imaging with computed tomography. Int. J. Cardiovasc. Imaging 24:411–421, 2008. [PubMed: 17955344]

15. Han HC Twisted blood vessels: symptoms, etiology and biomechanical mechanisms. J. Vasc. Res 49:185–187, 2012. [PubMed: 22433458]

16. Hiroki M, Miyashita K, and Oda M. Tortuosity of the white matter medullary arterioles is related to the severity of hypertension. Cerebrovasc. Dis 13:242–250, 2002. [PubMed: 12011548]

17. Huo Y, Wischgoll T, and Kassab GS. Flow patterns in three-dimensional porcine epicardial coronary arterial tree. Am. J. Physiol. Heart Circ. Physiol 293:H2959–H2970, 2007. [PubMed: 17827262]

18. Jakob M, Spasojevic D, Krogmann ON, Wiher H, Hug R, and Hess OM. Tortuosity of coronary arteries in chronic pressure and volume overload. Cathet. Cardiovasc. Diagn 38:25–31, 1996. [PubMed: 8722854]

19. Johnson K, Sharma P, and Oshinski J. Coronary artery flow measurement using navigator echo gated phase contrast magnetic resonance velocity mapping at 3.0 T. J. Biomech 41:595–602, 2008. [PubMed: 18036532]

20. Johnston BM, Johnston PR, Corney S, and Kilpatrick D. Non-Newtonian blood flow in human right coronary arteries: steady state simulations. J. Biomech 37:709–720, 2004. [PubMed: 15047000]

21. Johnston BM, Johnston PR, Corney S, and Kilpatrick D. Non-Newtonian blood flow in human right coronary arteries: transient simulations. J. Biomech 39:1116–1128, 2006. [PubMed: 16549100]

22. Joshi AK, Leask RL, Myers JG, Ojha M, Butany J, and Ethier CR. Intimal thickness is not associated with wall shear stress patterns in the human right coronary artery. Arterioscler. Thromb. Vasc. Biol 24:2408–2413, 2004. [PubMed: 15472129]

23. Katouzian A, Sathyanarayana S, Baseri B, Konofagou EE, and Carlier SG. Challenges in atherosclerotic plaque characterization with intravascular ultrasound (IVUS): from data collection to classification. IEEE Trans. Inf. Technol. Biomed 12:315–327, 2008. [PubMed: 18693499]

24. Kotys MS, Herzka DA, Vonken EJ, et al. Profile order and time-dependent artifacts in contrast-enhanced coronary MR angiography at 3T: origin and prevention. Magn. Reson. Med 62:292–299, 2009. [PubMed: 19526488]

25. Kubo T, Imanishi T, Takarada S, et al. Assessment of culprit lesion morphology in acute myocardial infarction: ability of optical coherence tomography compared with intravascular ultrasound and coronary angioscopy. J. Am. Coll. Cardiol 50:933–939, 2007. [PubMed: 17765119]

26. Lee SW, Antiga L, Spence JD, and Steinman DA. Geometry of the carotid bifurcation predicts its exposure to disturbed flow. Stroke 39:2341–2347, 2008. [PubMed: 18556585]

27. Lehoux S, Castier Y, and Tedgui A. Molecular mechanisms of the vascular responses to haemodynamic forces. J. Intern. Med 259:381–392, 2006. [PubMed: 16594906]

28. MacLean NF, and Roach MR. Thickness, taper, and ellipticity in the aortoiliac bifurcation of patients aged 1 day to 76 years. Heart Vessels 13:95–101, 1998. [PubMed: 9987643]

29. Malek AM, Alper SL, and Izumo S. Hemodynamic shear stress and its role in atherosclerosis. JAMA 282:2035–2042, 1999. [PubMed: 10591386]

30. Medina A, Suarez de Lezo J, and Pan M. A new classification of coronary bifurcation lesions. Rev. Esp. Cardiol 59(2):183–184, 2006. [PubMed: 16540043]

31. Murray CD The Physiological principle of minimum work: I. The vascular system and the cost of blood volume. Proc. Natl Acad. Sci. U.S.A 12:207–214, 1926. [PubMed: 16576980]

32. Nissen SE, Gurley JC, Grines CL, Booth DC, McClure R, Berk M, Fischer C, and DeMaria AN. Intravascular ultrasound assessment of lumen size and wall morphology in normal subjects and patients with coronary artery disease. Circulation 84(3):1087–99, 1991. [PubMed: 1884441]

33. Ong CW, Dokos S, Chan BT, Lim E, Al Abed A, Abu Osman NAB, Kadiman S, Lovell NH. Numerical investigation of the effect of cannula placement on thrombosis. Theor. Biol. Med. Model 2013:10–35, 2013.

34. Pancera P, Ribul M, Presciuttini B, Lechi A. Prevalence of carotid artery kinking in 590 consecutive subjects evaluated by echo-color Doppler. Is there a correlation with arterial hypertension? J. Intern. Med 248:7–12, 2000. [PubMed: 10947875]

35. Rioufol G, Gilard M, Finet G, Ginon I, Boschat J, and Andre-Fouet X. Evolution of spontaneous atherosclerotic plaque rupture with medical therapy: long-term follow-up with intravascular ultrasound. Circulation 110:2875–2880, 2004. [PubMed: 15492303]

36. Sankaranarayanan M, Chua LP, Ghista DN, and Tan YS Computational model of blood flow in the aorto-coronary bypass graft. Biomed. Online 4:1–14, 2005.

37. Sanz J, and Fayad ZA. Imaging of atherosclerotic cardiovascular disease. Nature 451:953–957, 2008. [PubMed: 18288186]

38. Soulis JV, Farmakis TM, Giannoglou GD, and Louridas GE. Wall shear stress in normal left coronary artery tree. J. Biomech 39:742–749, 2006. [PubMed: 16439244]

39. Stone PH, Coskun AU, Kinlay S, et al. Effect of endothelial shear stress on the progression of coronary artery disease, vascular remodeling, and in-stent restenosis in humans: in vivo 6-month follow-up study. Circulation 108:438–444, 2003. [PubMed: 12860915]

40. Tearney GJ, Waxman S, Shishkov M, et al. Three-dimensional coronary artery microscopy by intracoronary optical frequency domain imaging. JACC Cardiovasc. Imaging 1:752–761, 2008. [PubMed: 19356512]

41. Thomas JB, Antiga L, Che SL, et al. Variation in the carotid bifurcation geometry of young versus older adults: implications for geometric risk of atherosclerosis. Stroke 36:2450–2456, 2005. [PubMed: 16224089]

42. Thomas JB, Milner JS, and Steinman DA. On the influence of vessel planarity on local hemodynamics at the human carotid bifurcation. Biorheology 39:443–448, 2002. [PubMed: 12122265]

43. van Wyk S, Prahl Wittberg L, and Fuchs L. Wall shear stress variations and unsteadiness of pulsatile blood-like flows in 90-degree bifurcations. Comput. Biol. Med 43: 1025–1036, 2013. [PubMed: 23816175]

44. van Wyk S, Prahl Wittberg L, and Fuchs L. Atherosclerotic indicators for blood-like fluids in 90-degree arterial-like bifurcations. Comput. Biol. Med 50:56–69, 2014. [PubMed: 24835086]

45. Weibel J, and Fields WS. Tortuosity, coiling, and kinking of the internal carotid artery. I. Etiology and radiographic anatomy. Neurology 15:7–18, 1965. [PubMed: 14257832]

46. Wellnhofer E, Goubergrits L, Kertzscher U, Affeld K, and Fleck E. Novel non-dimensional approach to comparison of wall shear stress distributions in coronary arteries of different groups of patients. Atherosclerosis 202:483–490, 2009. [PubMed: 18617176]

47. Wellnhofer EJ, Kertzscher U, Affeld K, Fleck E, and Goubergrits L Non-dimensional modeling in flow simulation studies of coronary arteries including side-branches: a novel diagnostic tool in coronary artery disease. Atherosclerosis 216:277–282, 2011. [PubMed: 21333992]

48. Zakaria H, Robertson AM, and Kerber CW. A parametric model for studies of flow in arterial bifurcations. Ann. Biomed. Eng 36:1515–1530, 2008. [PubMed: 18629648]

49. Zeng D, Ding Z, Friedman MH, and Ethier CR. Effects of cardiac motion on right coronary artery hemodynamics. Ann. Biomed. Eng 31:420–429, 2003. [PubMed: 12723683]

50. Zhu H, Ding Z, Piana RN, Gehrig TR, and Friedman MH. Cataloguing the geometry of the human coronary arteries: a potential tool for predicting risk of coronary artery disease. Int. J. Cardiol 135:43–52, 2009. [PubMed: 18597872]
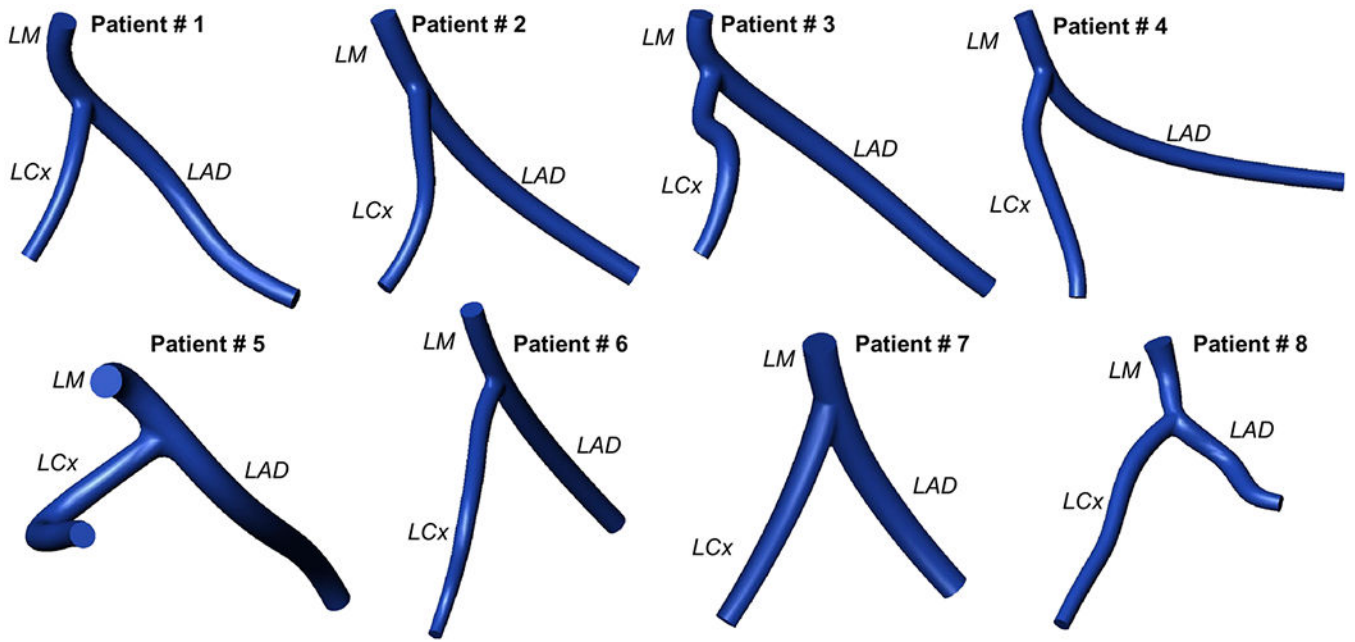
FIGURE 1.
3D reconstructed geometries of the left main coronary bifurcations based on CT scans of eight patients.
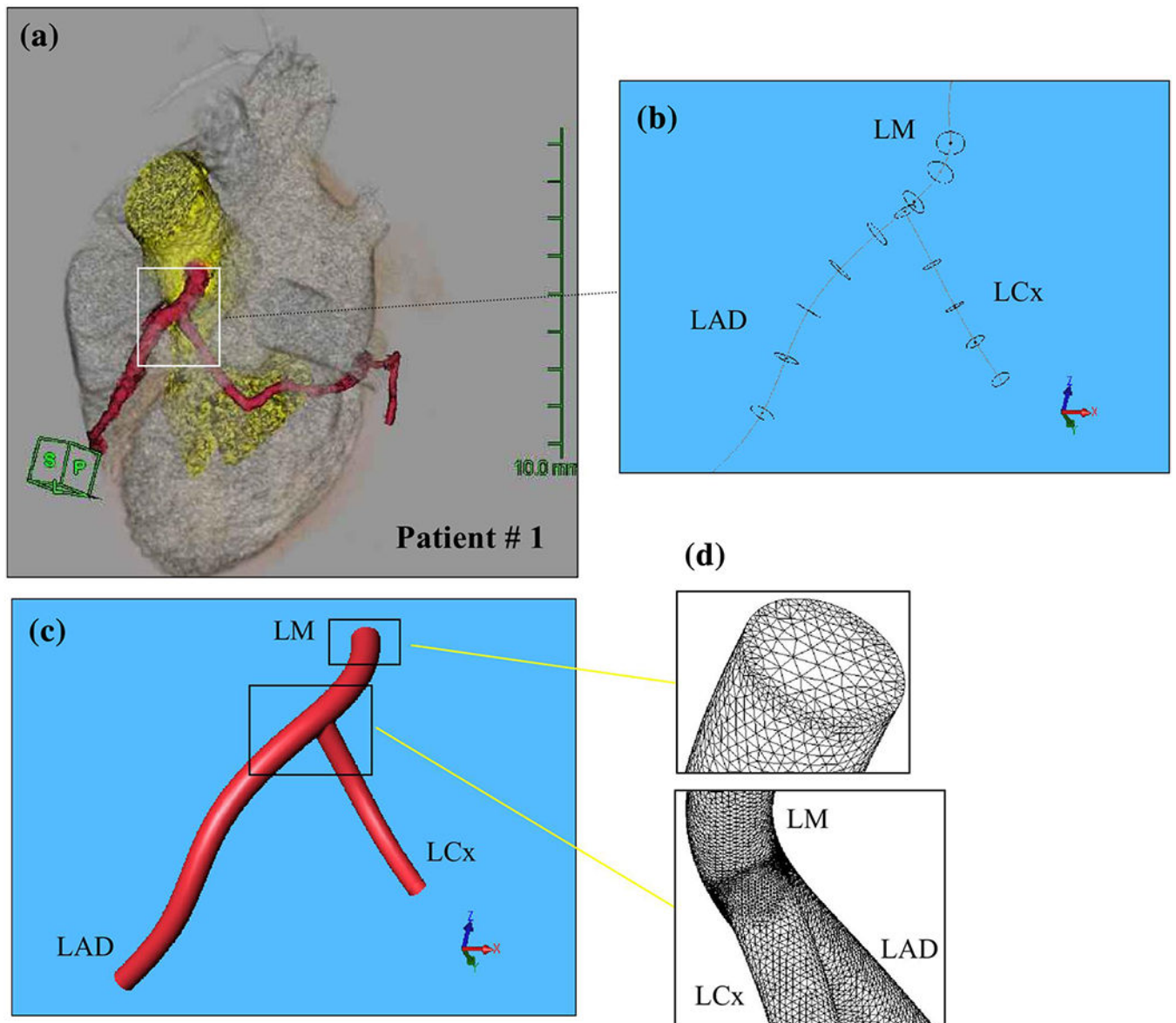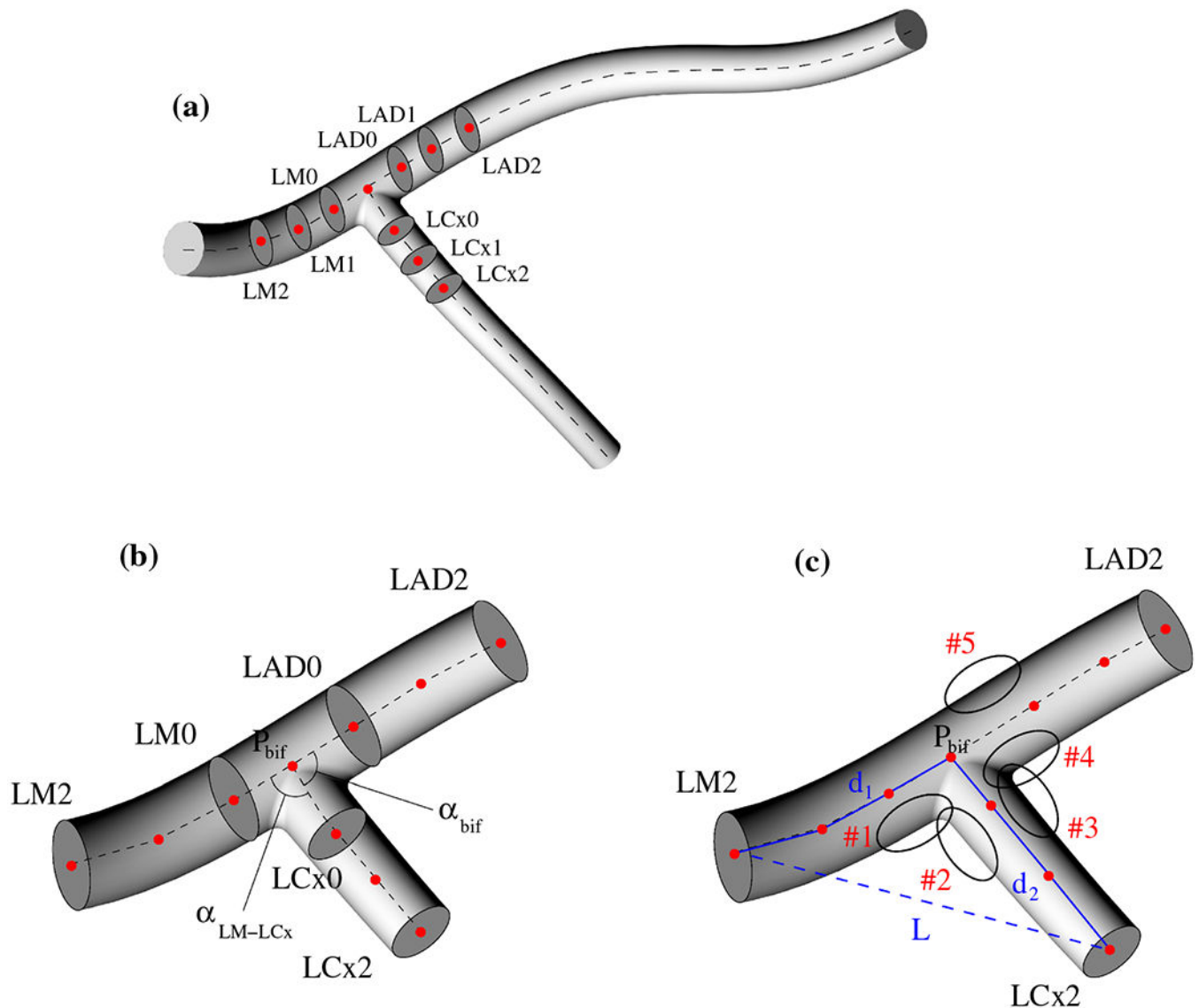
FIGURE 2.
3D reconstruction of the coronary bifurcation. (a) CT view of the left main coronary bifurcation. The square indicates the studied region. (b) Illustrations of the circular cross-sectional lumen areas and centerlines of the LM, LAD and LCx branches used for the 3D reconstruction. (c) Resulting b-spline surface used for the CFD. (d) Numerical grid used for CFD simulations performed on the left main coronary bifurcation of the Patient #1.

FIGURE 3.
Definition of geometric parameters. (a) Reconstructed coronary bifurcation of Patient #1 used for the CFD simulations. (b) Associated restricted geometry used to define the geometric indexes. (c) Locations of the five regions of interest (region #1–5) in which the WSS amplitudes were obtained. Regions #1, 3 and 4 are sites of high WSS while region #2 and 5 are sites of low WSS. The tortuosity of the LM2+LCx2 coronary artery segment is given by the ratio $100 \times (d - L)/L$, where $d = d1 + d2$ is the total length of the coronary artery segment and L is the shortest distance.
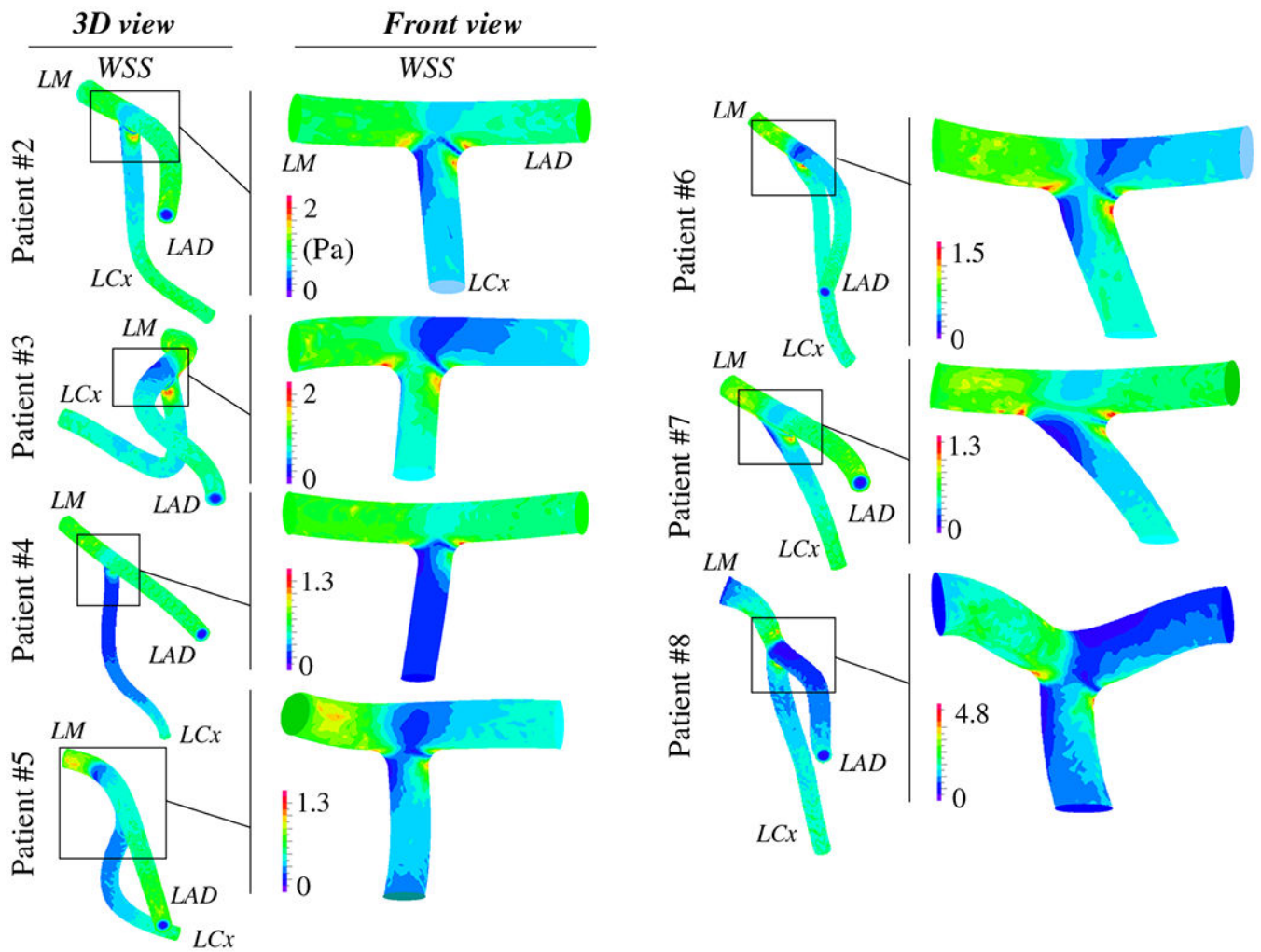
FIGURE 4.
Front views showing the spatial distributions of the computed WSS (unit: Pa) at the level of the restricted left main coronary bifurcation model of each patient. The 3D views of the coronary bifurcations highlighting both the tortuosities of the arterial branches and the spatial distributions of the WSS are visible in the first column.

FIGURE 5.
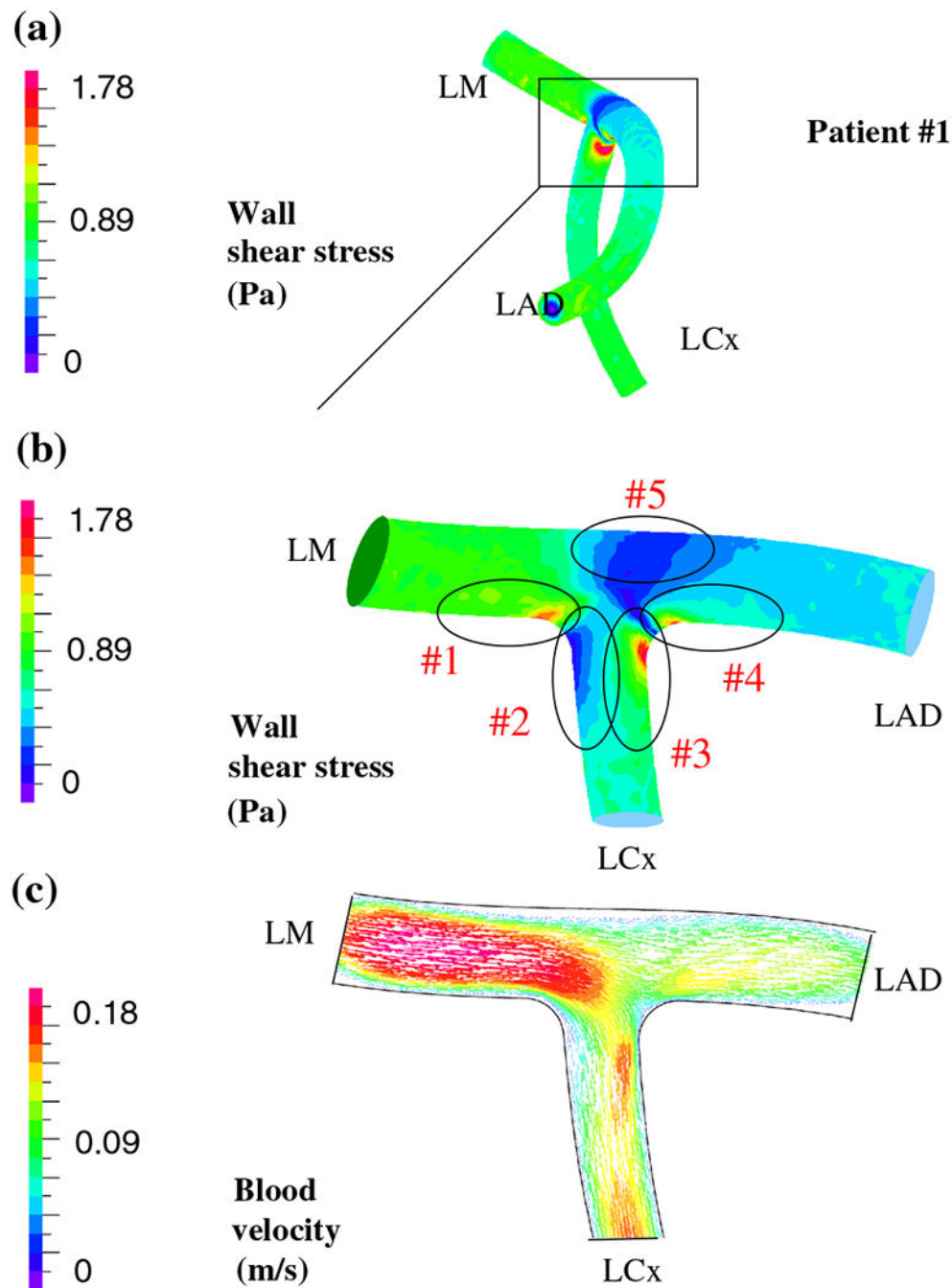
Results highlighting the spatial distributions of WSS (unit: Pa) (a, b) and blood velocity field (unit: m/s) (c) at the level of the left main coronary bifurcation of Patient #1. The circles indicate the five sites of interest where WSS amplitudes where collected (regions #1–5, illustrated also in Fig. 3c). Regions #1, 3 and 4 are sites of high WSS while region #2 and 5 are sites of low WSS.

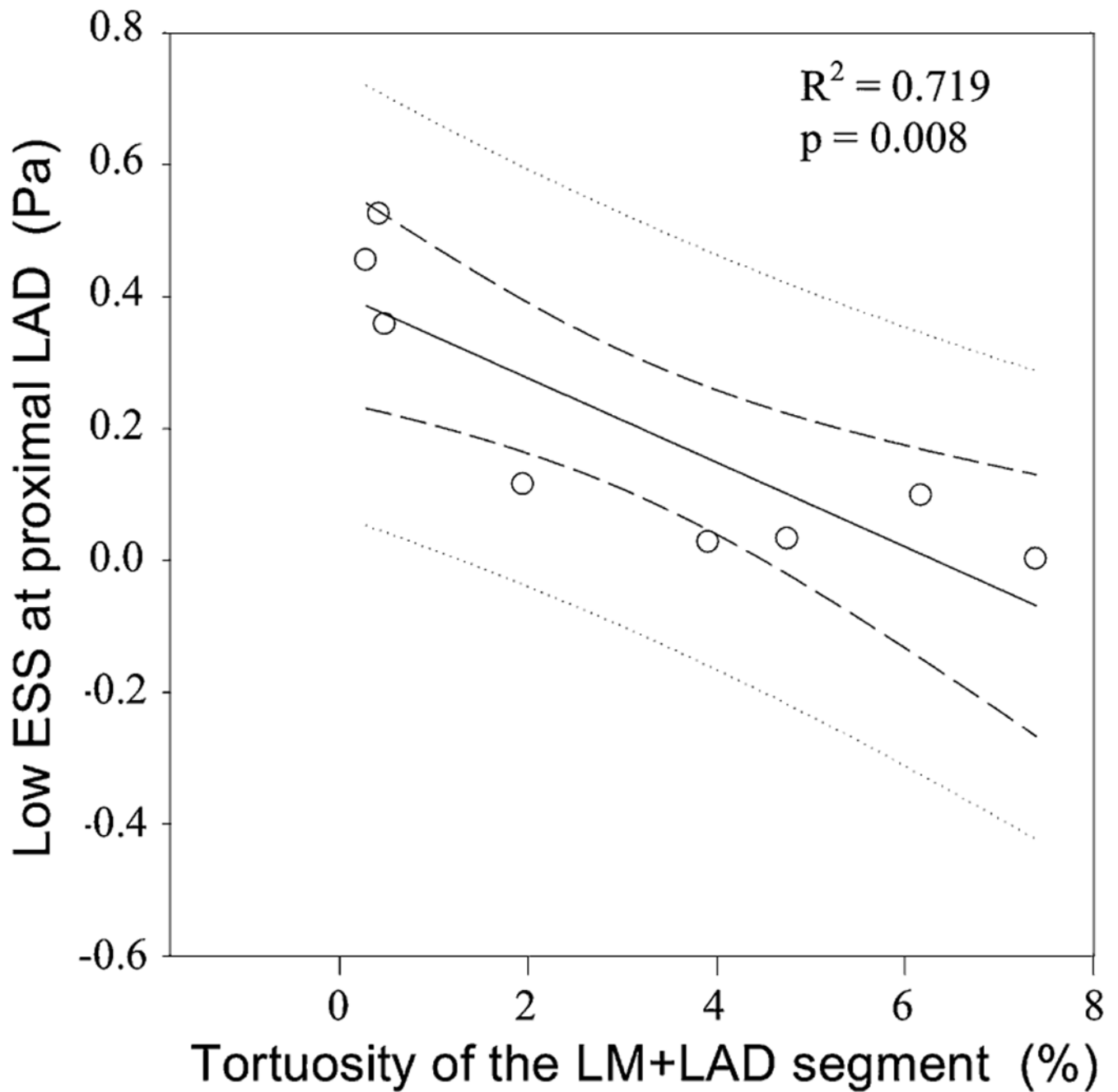**FIGURE 6.**
Strong linear correlations found between the low amplitude of the WSS at the proximal LAD region opposite to the flow divider (low-WSS_{LAD}) and the tortuosity index of the LM +LAD arterial segment ($Tortuosity_{LM–LAD}$). The confidence and prediction intervals (area between the internal and external dashed lines, respectively) were also plotted.

TABLE 1.

Measured geometric indexes and plaque locations of the eight studied coronary bifurcations explored by CT scans.

Patient #	1	2	3	4	5	6	7	8	Mean ± SD
Diameter$_{LM}$ (mm)	4.7	4.76	4.28	4.53	3.94	4.21	5.5	6	–
Diameter$_{LAD}$ (mm)	3.765	3.378	3.48	4.8	2.9	3.66	4.76	3.5	–
Diameter$_{LCx}$ (mm)	3.24	3.05	3.45	2.72	3.587	3.8	3.64	3.4	–
Tortuosity$_{LM-LAD}$ (%)	3.91	0.42	4.75	0.28	6.17	1.95	0.48	7.39	3.17 ± 2.79
Tortuosity$_{LM-LCx}$ (%)	30	31.62	51.31	44.45	35.86	16.74	6.83	16.78	29.20 ± 15.03
Tortuosity$_{LAD-LCx}$ (%)	52.45	49.26	35.80	28.41	39.70	60.35	135.49	35.42	54.61 ± 34.31
AR$_{LAD-LM}$ (%)	97.32	82.65	72.95	92.57	119.11	105.29	97.10	83.19	93.77 ± 14.49
AR$_{LCX-LM}$ (%)	60.11	61.06	69.38	63.33	83.49	88.03	58.74	75.54	69.96 ± 11.26
α$_{bif}$ (°)	88.50	84.39	93.50	101.01	79.81	75.22	44.07	87.29	81.72 ± 17.15
α$_{LM-LCx}$ (°)	96.54	96.38	83.70	81.66	106.83	110.35	140.27	117.25	104.12 ± 19.14
α$_{LM-LAD}$ (°)	172.31	175.91	172.69	177.24	171.87	173.69	175.39	153.39	171.56 ± 7.58
Plaque at LM, LAD, LCx	(1,1,1)	(0,1,1)	(1,1,0)	[*]	(1,1,1)	(1,1,1)	(1,0,0)	(1,1,1)	—

AR$_{LAD/LM}$ and AR$_{LCx/LM}$ are the area ratios LAD/LM and LCx/LM, respectively. α$_{bif}$ is the bifurcation angle (i.e., the angle between LCx and LAD segments). α$_{LM-LCx}$ and α$_{LM-LAD}$ are the angles between the LM and LCx segments and LM and LAD segments, respectively. The symbol * indicates that clinical plaque location examination was not performed for this patient. The Medina classification of bifurcation lesions was used[30] (where 1 and 0 indicate the presence and absence of plaque, respectively).

TABLE 2.

Correlations between WSS amplitudes.

	Pearson product moment correlation			
	Low-WSS$_{LAD}$	High-WSS$_{LM}$	High-WSS$_{LCx}$	High-WSS$_{LAD}$
Low-WSS$_{LCx}$	0.123	0.044	0.025	0.0125
	NS (0.394)	NS (0.618)	NS (0.707)	NS (0.391)
Low-WSS$_{LAD}$		0.202	0.213	0.119
		NS (0.264)	NS (0.251)	NS (0.402)
Low-WSS$_{LM}$			0.920	0.939
			<0.0002	<0.0002
Low-WSS$_{LCx}$				0.931
				<0.0002

Pearson product moment correlation between the amplitudes of the WSS calculated at the five sites of interest illustrated in Fig. 3c (namely the low-WSS$_{LAD}$, low-WSS$_{LCx}$, high-WSS$_{LCx}$, high-WSS$_{LM}$, high-WSS$_{LAD}$ and high-WSS$_{LCx}$ amplitudes). Each cell contains first the correlation coefficient R^2 and second the p value. NS = Non Significant.

TABLE 3.

Correlations between WSS amplitudes and bifurcation angles.

	Model coefficient of the multiple linear regression					
	R^2	p	α_{bif}	p	α_{LM-LCx}	p
Low-WSS$_{LCx}$	0.437	NS (0.238)	-5.77×10^{-4}	NS (0.302)	-7.73×10^{-4}	NS (0.146)
Low-WSS$_{LAD}$	0.189	NS (0.593)	-1.25×10^{-2}	NS (0.332)	-1.06×10^{-2}	NS (0.356)
High-WSS$_{LM}$	0.803	0.017	0.150	0.007	0.134	0.007
High-WSS$_{LCx}$	0.732	0.037	0.124	0.015	0.111	0.016
High-WSS$_{LAD}$	0.851	0.009	0.095	0.003	0.086	0.003

Multiple regressions of WSS amplitudes calculated at the five sites of interest illustrated in Fig. 3c (namely the low-WSS$_{LAD}$, low-WSS$_{LCx}$, high-WSS$_{LM}$, high-WSS$_{LAD}$ and high-WSS$_{LCx}$ amplitudes), with the bifurcation angles as geometric factors predictors. α_{LM-LCx} is the angle between the LM and LCx segments. α_{bif} is the bifurcation angle (i.e., the angle between the LAD and LCx segments).